The reaction of sulfur dioxide radical cation with hydrogen and its relevance in solar geoengineering models

Mauro Satta,[*,†] Antonella Cartoni,[*,‡] Daniele Catone,[¶] Mattea Carmen Castrovilli,[§] Paola Bolognesi,[§] Nicola Zema,[¶] and Lorenzo Avaldi[§]

†*ISMN (CNR) c/o Dipartimento di Chimica Sapienza Università di Roma, Pl.e Aldo Moro 5, Roma, Italy*

‡*Dipartimento di Chimica, Sapienza Università di Roma, Pl.e Aldo Moro 5, Roma, Italy*

¶*CNR-ISM, Area della Ricerca di Tor Vergata, Via del Fosso del Cavaliere, Roma, Italy*

§*CNR-ISM, Area della Ricerca di Roma 1, Via Salaria Km 29,300, Monterotondo Scalo (RM), Italy*

E-mail: mauro.satta@cnr.it; antonella.cartoni@uniroma1.it

Abstract

Sulfur dioxide has been proposed in solar geoengineering as a precursor of H_2SO_4 aerosol, a cooling agent active in the stratosphere to contrast climate change due to the anthropogenic emissions of greenhouse carbon dioxide. Atmospheric ionization sources can ionize SO_2 into excited states of $SO_2^{\cdot+}$ radical cation, which quickly reacts with trace gases in the stratosphere. In this work we explore the reaction of $H_2(D_2)$ with $SO_2^{\cdot+}$ ions excited by tunable synchrotron radiation. The experimental results show that the reactivity decreases as the photon energy increases, and that $HSO_2^+ + H$ ($DSO_2^+ + D$) are the ionic and neutral products, where the hydrogen atom is an important agent

of ozone depletion leading to OH and O_2. Density Functional Theory and Variational Transition State Theory have been used to investigate the dynamics of the title reaction, which is barrierless and exothermic by 75.5 kJ/mol with a rate coefficient $k = 2.9 \cdot 10^{-11}$ cm^3 molecule^{-1} s $^{-1}$ at 300 K. Spin and charge effects have been analyzed to clarify the reaction dynamics. In order to explain the experimental trend of the reaction an effective temperature is defined to properly account for the non-thermal energy dynamics. The present results suggest that solar geoengineering models should test the reactivity of $SO_2^{\cdot+}$ with major trace gases in the stratosphere, especially H_2 and H_2O ($SO_2^{\cdot+} + H_2O \rightarrow HSO_2^+ + OH$) since both reactions are pathways to the formation of OH, which in turn oxides SO_2, starting the chemical reactions leading to H_2SO_4 aerosol formation. These reactions should be considered as relevant channels to the OH formation especially during the nighttime when there is not OH production by sunlight.

Introduction

Technologies that aim to cool the planet by partially reflecting sunlight away from Earth back into space are the core of the solar geoengineering[1–5]. These technologies, which aim to manipulate the atmosphere to fight climate change, have triggered an active discussion[6–9] even at the level of the highest international institutions, such as the United Nations Environment Assembly[10,11]. The goal of solar geoengineering is to artificially reduce global temperatures by sunlight-reflecting particles generated in the atmosphere mainly by sulfur dioxide, which would be injected in the stratosphere to contrast global climate warming[8]. The idea is that this strategy should mimic the effects of the natural emission of sulfur dioxide by volcanic eruption. Nevertheless, several worries have been raised about the long-term consequences of these technologies on the ozone-layer[7], on the unbalances of the water cycle, i.e. droughts and/or floods[12], or even on the biodiversity threats[13]. Up to now, almost only theoretical models have been used to predict the right amount of the cooling agent necessary to produce

a climate cooling without a severe irreversible alteration of the global climate[6]. The present models take into account several neutral molecules, their thermal reactions and photoinduced dissociation[14]. However, ion-molecule reactions may also play a relevant role in the chemical transformation of several species since, especially in the stratosphere, ionizing radiation are not negligible and much effort has been paid to determine the amount and nature of these radiation produced by cosmic rays and space weather events in the atmosphere[15–20]. Typical average values of the neutral/ion ratio during daytime at mid-latitudes in the stratosphere is about 10^{12}, and it is independent by the type of molecular species because cosmic rays ionize all neutral molecules in the stratosphere with a similar efficiency[19]. This low ion/neutral ratio can be counterbalanced by the fact that ion-molecule reactions are generally much faster then the neutral-neutral reactions (i.e. the neutral chemistry involved in the conversion of SO_2 into H_2SO_4 takes approximately 30 days[21]), and can heavily alter the total budget of important molecular species in the atmosphere. Hence, reactions involving the radical cation $SO_2^{\cdot+}$, which can be produced in the stratosphere by ionizing radiation, should be considered in the chemistry models used when evaluating the climate impact of solar geoengineering involving sulfur dioxide as aerosol precursor. The role of the ionizing radiation on the SO_2 geoengineering release in the stratosphere should be deeply considered also in view of the fact that during natural volcanic emission of sulfur dioxide large amount of particulates are also emitted. These can largely absorb the ionizing radiation, and thus reduce the natural production of $SO_2^{\cdot+}$. This radiation "shield" effect obviously will not act when only gaseous SO_2 is injected by balloons or aircrafts to artificially produce aerosol particulates. This aspect should be considered when comparison between sulfur dioxide volcanic and geoengineering emission are discussed as similar processes.

Moreover, the non-thermal conditions, under which the ion-molecule reactions in the stratosphere can occur, should also be taken into account. The ionizing radiation produces highly excited ions, which slowly thermalize with the surrounding molecular species in thermal equilibrium in the stratosphere[22–25]. These non-thermal effects are generally amplified

for reactions between hot molecular ions and rigid neutral species with high vibrational frequencies[26,27]. Hence, we have explored the reaction between the radical cation $SO_2^{\cdot+}$ and the H_2 molecule (eq 1), one of the major trace gas in the stratosphere (about 0.5 ppmv[28]) with almost constant concentration with the altitude.

This work follows recent studies on ion-molecule reactions[29–32], and on the dynamic of the Hydrogen Atom Transfer (HAT) reaction of sulfur dioxide radical cation $SO_2^{\cdot+}$ with methane and water leading to HSO_2^+ ions[33] and CH_3 or OH, which is a relevant oxidant in the environmental chemistry[34,35]. The ionic product of these reactions, HSO_2^+ has been detected in the terrestrial stratosphere with other sulfur oxides protonated species[36] and reacts with water via proton transfer[33]. The title reaction (eq 1) has been studied experimentally using tunable synchrotron radiation to produce $SO_2^{\cdot+}$ in the excited ro-vibrational levels of the ionic ground state:

$$SO_2^{\cdot+} + H_2 \rightarrow HSO_2^+ + H \tag{1}$$

In the stratosphere one of main chemical process involving H is the reaction with ozone leading to molecular oxygen and hydroxyl radical:

$$H + O_3 \rightarrow O_2 + OH \tag{2}$$

Eq 2 has a rate coefficient[14] of $2.89 \cdot 10^{-11}$ cm^3 molecule^{-1} s $^{-1}$, and it is both a chemical route for the destruction of ozone and a source of OH. Eq 1 and eq 2, together with the efficient reaction of $SO_2^{\cdot+}$ with water[33], is a nighttime alternative pathway to the sunlight formation of OH[14]. The latter can oxidize SO_2, and trigger the chemical reactions network leading to the formation of H_2SO_4 aerosol in the stratosphere, which in turn could modify the expected size distribution of the particulates with consequences on the global expected cooling effects. It is noteworthy that another largely studied oxidant species in the troposphere are the Criegee Intermediates (CI)[37]. However, in the stratosphere the role of the CI

in the oxidation chemistry is not so relevant due to the hereby low concentration of organic compounds, and to the low pressures that hinder the stabilization of the CI[38].

The experiments performed in this work have been supported by a theoretical exploration of the reaction dynamics on the potential energy surface with Density Functional Theory (DFT) and Variational Transition State Theory (VTST)[39,40]. The spin and charge effects, as well as Ionization Energy (IE), polarizability, binding energy, radical stability and ro-vibrational degrees of freedom along the reaction path, have been also considered to explain the dynamics of the reaction. The same study has been performed also with the D_2 molecule, and a comparison with the reaction of $SO_2^{\cdot+}$ with water and methane, as well as other previous ion-molecule reaction studies of $SO_2^{\cdot+}$ and $CH_4^{\cdot+}$ with hydrogen, has been carried out[26,33,41,42]. All along the manuscript the radical symbol in $SO_2^{\cdot+}$ has been omitted for the sake of simplicity.

Results and Discussion

Synchrotron Experiments. The measurements were carried out at the "Circular Polarization" beamline (CiPo) of ELETTRA synchrotron (Trieste, Italy)[43] with the setup operated at the room temperature and described in the experimental section. The SO_2^+ ions were obtained at low pressure (about 10^{-6} mbar) from the ionization of an effusive molecular beam of SO_2 by monochromatic synchrotron radiation tuned in the photon energy range 12.4-15.0 eV. The SO_2^+ thus can be produced in the ground X^2A_1 state (IE=12.349 eV) or in the two excited electronic states: the $^2B_2$ (12.988 eV) and $^2A_2$ (13.338 eV) ones, very close in energy[44,45]. However, as already well established[33], the electronically excited states of SO_2^+ ion decay to excited ro-vibrational states of the ground electronic state on a nanosecond timescale before the reaction with the neutral (H_2/D_2) occurs (timescale fraction of ms). In this way the reacting SO_2^+ ions are "hot", with an internal energy increasing as the photoionizing energy is increased, and it is not in thermal equilibrium with the environment at room

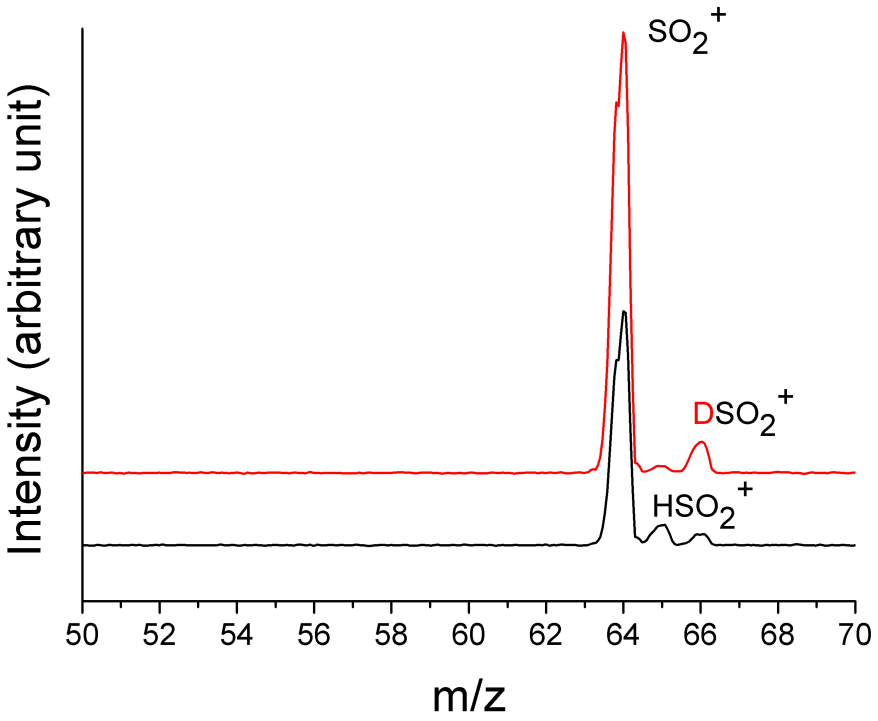

Figure 1: Mass spectra recorded at the photon energy 14.0 eV, nominal CE=0.0 eV and P = $5.1 \cdot 10^{-5}$ and $8.0 \cdot 10^{-5}$ mbar for the reaction with H_2 (black line) and D_2 (red line), respectively.

temperature. Moreover, the mass spectra acquired in the photon energy range 12.4-15.0 show that the SO_2^+ ions do not dissociate, as also demonstrated by photoelectron-photoion coincidence (PEPICO) measurements[33,46], and no reaction with the residual water in the octupole (base pressure about 10^{-7} mbar) was observed. The SO_2^+ ions were guided in the reaction zone (octupole) at the nominal Collision Energy (CE) of 0.0 eV with an estimated energy spread of 0.1 eV. Neutral gas H_2/D_2 was introduced in the octupole at the room temperature via a controlled needle valve at the pressure of about 10^{-5} mbar. The experiments were performed at different photon energy, pressure and CE by changing one parameter at the time. The yields of the ionic reagent and products were recorded and their ratio was analyzed. The mass spectra acquired at the photon energy 14.0 eV for the ion-molecule reaction between SO_2^+ and H_2/D_2 are shown in Figure 1.

The mass spectra were acquired at pressure of $5.1 \cdot 10^{-5}$ and $8.0 \cdot 10^{-5}$ mbar for neutral

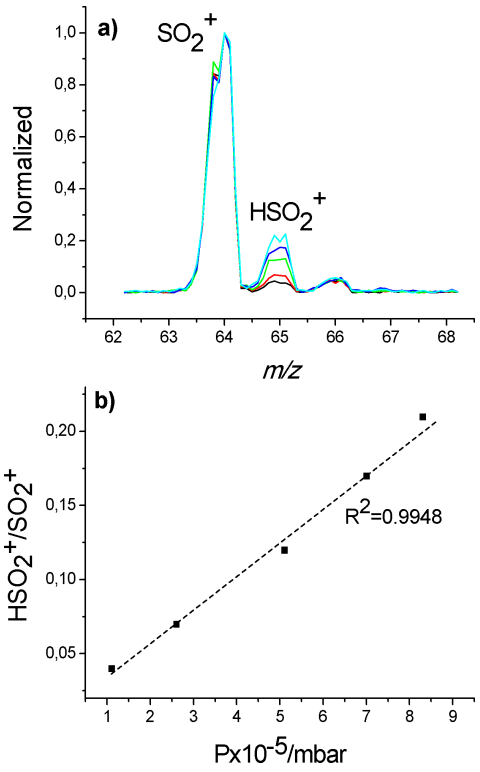

Figure 2: a) The mass spectrum in the region of 62<m/z<68 acquired at the photon energy 14.0 eV, nominal CE=0.0 eV and pressures of H_2: $1.1 \cdot 10^{-5}$ mbar (black line), $2.6 \cdot 10^{-5}$ mbar (red line), $5.1 \cdot 10^{-5}$ (green line), $7.0 \cdot 10^{-5}$ (blue) and $8.3 \cdot 10^{-5}$ (light blue) mbar. The intensities are normalized to that of the reagent ion. SO_2 pressure in the ion source was $4.4 \cdot 10^{-6}$ mbar; b) HSO_2^+/SO_2^+ ratio as a function of the H_2 pressure.

H_2 and D_2, respectively. In the case of the H_2 as reagent (black line in Figure 1), a peak at m/z 65 (HSO_2^+) is observed with a signal of about 11% relative to the most intense peak SO_2^+ m/z 64. In the case of reaction with deuterium (red line in Figure 1) a peak at m/z 66 (DSO_2^+) is observed with an intensity of about 8% of the most intense peak SO_2^+ at m/z 64 (see experimental section).

In Figure 2a the mass spectra of the $SO_2^+ + H_2$ reaction, acquired at the photon energy of 14.0 eV and as a function of the H_2 pressure are shown. The peaks intensity of the ions at m/z 65 is normalized with respect to the SO_2^+ peak at m/z 64. As expected an increase of m/z 65 signal is observed relative to all other peaks when the pressure varies from $1.1 \cdot 10^{-5}$ to $8.3 \cdot 10^{-5}$ mbar. The trend of the ion intensity ratio (HSO_2^+/SO_2^+) vs nominal pressure of H_2 (Figure 2b) demonstrates that the HSO_2^+ is produced by reaction (1). Afterwards,

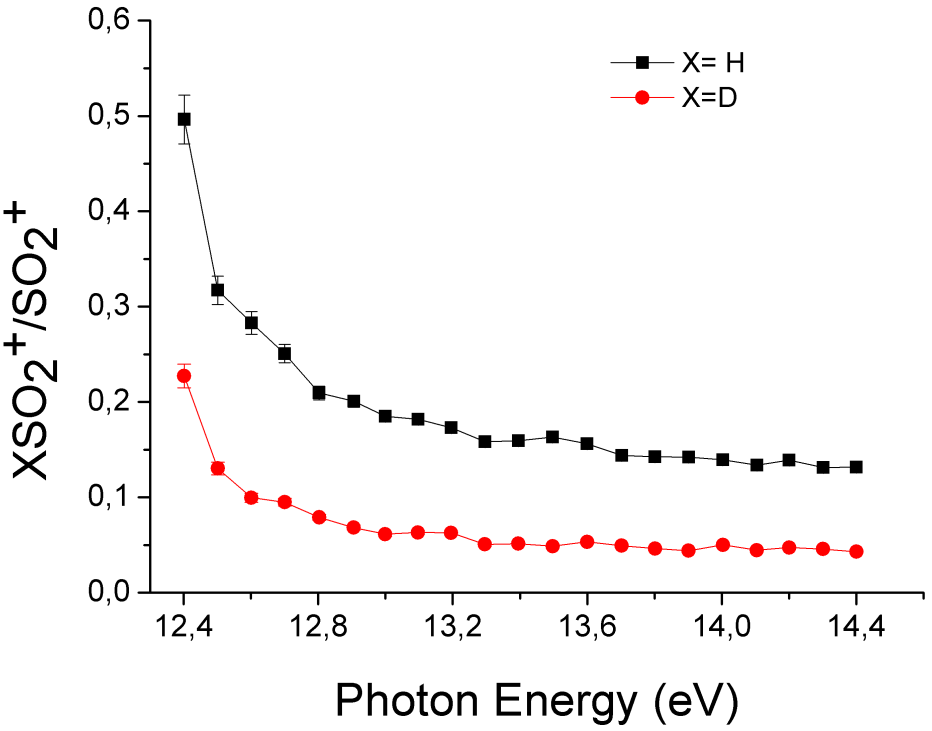

Figure 3: $H(D)SO_2^+/SO_2^+$ ratio as a function of photon energy in the reaction of SO_2^+ with H_2 (black line) and D_2 (red line) at the fixed pressure of neutrals of $8.3 \cdot 10^{-5}$ mbar and nominal CE=0.0 eV

the yields of SO_2^+ and $H(D)SO_2^+$ ions were acquired at fixed pressures of the neutral H_2/D_2 and at the nominal CE=0.0 eV varying the photon energy from 12.4 to 15.0 eV. The ratio $H(D)SO_2^+/SO_2^+$ for both reactions at the nominal fixed pressure of about $8.3 \cdot 10^{-5}$ mbar as a function of photon energy is reported in Figure 3.

The results clearly show that as the internal energy of SO_2^+ increases the ratio $H(D)SO_2^+/SO_2^+$ decreases, is higher in the H case, and the observed isotopic effect demonstrates the main role of hydrogen in the reaction coordinate. Furthermore, the ratio HSO_2^+/SO_2^+ decreases at increasing nominal CE from 0.0 to 1.2 eV at fixed photon energy (Figure S1 in SI). Thermochemical literature data of reactants and products of reaction (1) show that the HAT reaction is exothermic by 75.0 kJ/mol[48]. The literature data on experimental rate coefficients are referred to different experimental mass spectrometric techniques: in Selected Ion Flow Tube Mass Spectrometry (SIFT-MS) experiments the values of $4.2 \cdot 10^{-12} \pm 20\%$

Table 1: Bond Dissociation Energy (BDE), Ionization Energy (IE), dipole moment (μ) and polarizability (α) for H_2, H_2O and CH_4 molecules.[47]

	BDE (kJ/mol)	IE (eV)	μ (D)	α (Å^3)
H_2	435.58±0.01	15.42593±0.00005	//	0.787
H_2O	496.7±0.3	12.621±0.002	1.8550±0.0004	1.501
CH_4	438.9±0.1	12.61±0.01	//	2.448

and $5.0 \cdot 10^{-12} \pm 20\%$ cm^{3}molecule^{-1}s^{-1} were obtained[41,42] at 300 K, while a value of $1.7 \cdot 10^{-11} \pm 40\%$ cm^{3}molecule^{-1}s^{-1} was measured from the Fourier Transform Ion Cyclotron Resonance (FT-ICR) experiments at 298 K[49]. Although the values are quite different for SIFT and FT-ICR experiments, they are all lower than the Langevin rate coefficients[50,51] of $1.50 \cdot 10^{-9}$ or $1.53 \cdot 10^{-9}$ cm^{3}molecule^{-1}s^{-1}. Actually, many H-atom abstraction reactions involving H_2 are very slow[49]. In the specific case of the reaction involving $SO_2^+ + H_2$ a barrier of 19.9 kJ/mol has been found by early theoretical and experimental studies that account for the low rate coefficient at 300 K[41]. This evidence can not be only a consequence of the $H-H$ binding energy since the HAT reactions of SO_2^+ with CH_4 and H_2O are faster even if the $C-H$, $O-H$, $H-H$ molecular Bond Dissociation Energies (BDE) are comparable (Table 1)[52,53].

Minimum Energy Path (MEP). In order to explore the main factors affecting the reaction dynamics of the HAT from H_2 to SO_2^+ a theoretical study has been carried out by combining DFT and VTST approaches[54]. DFT was used to investigate the MEP of the reaction and to identify possible transition states and minima along the reactive coordinate, while VTST has been used to search for the "bottleneck" of the reaction, namely the Variational Transition State (**VTS**) configuration.

In Figure 4 the MEP of the reaction is shown. The reaction is barrierless and exothermic by 75.5 kJ/mol at 300 K with a minimum energy reaction complex configuration $[OSOH \cdots H]^+$ **Min** at 85.0 kJ/mol in cis conformation (See Table 2 for details on the geometric parameters of the molecular adducts whose atomic labels are defined in Figure 5).

The calculated exothermicity is in agreement with experimental value of 75.0 kJ/mol[48],

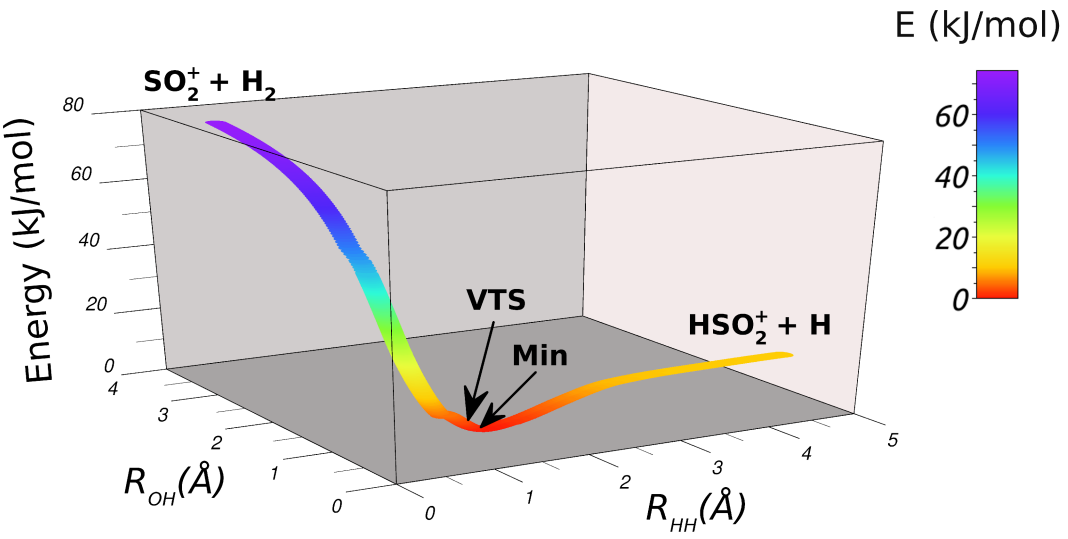

Figure 4: Minimum Energy Path for the $SO_2^+ + H_2$ reaction. The minimum energy of the complex $[OSOH \cdots H]^+$ is fixed at 0.0 kJ/mol. See the main text for further details.

and no transition state configuration was found above the energy of the reactants. Furthermore, the VTST approach identifies a **VTS** configuration $[O_dSO_cH_b \cdots H_a]^+$ along the MEP very close to **Min**, with similar geometry, charge and spin distribution (See Table 2 and Figure 5).

In both **VTS** and **Min** configurations the main bonds involved in the reaction, $O_c - H_b$ (about 1.0 Å) and $H_a - H_b$ (about 1.6 Å) are almost formed and fully stretched, respectively. In these configurations the charge ($H_bSO_2^+$: 0.90 e) and the spin (H_a: 0.85 $\hbar$) are almost fully localized as in the two final product moieties (see Figure 5). This dynamical picture seems very similar to that observed in the reaction of SO_2^+ with H_2O (see Figure 5 of Cartoni et al.[33]). However, through a careful analysis of the reaction it can be seen that

Table 2: Geometrical parameters for the main molecular species relevant to the title reaction. Distances in Å and angles in degrees.

	$R_{H_a-H_b}$	$R_{O_c-H_b}$	R_{S-O_c}	R_{S-O_d}	$\theta_{O_cSO_d}$	$\theta_{SO_cH_b}$	$\theta_{O_cH_bH_a}$
Reagents	0.75	//	1.46	1.46	130.4	//	//
VTS	1.59	1.02	1.56	1.44	115.1	122.4	171.2
Min	1.61	1.01	1.56	1.44	115.1	122.4	171.2
Products	//	0.99	1.56	1.44	114.9	121.2	//

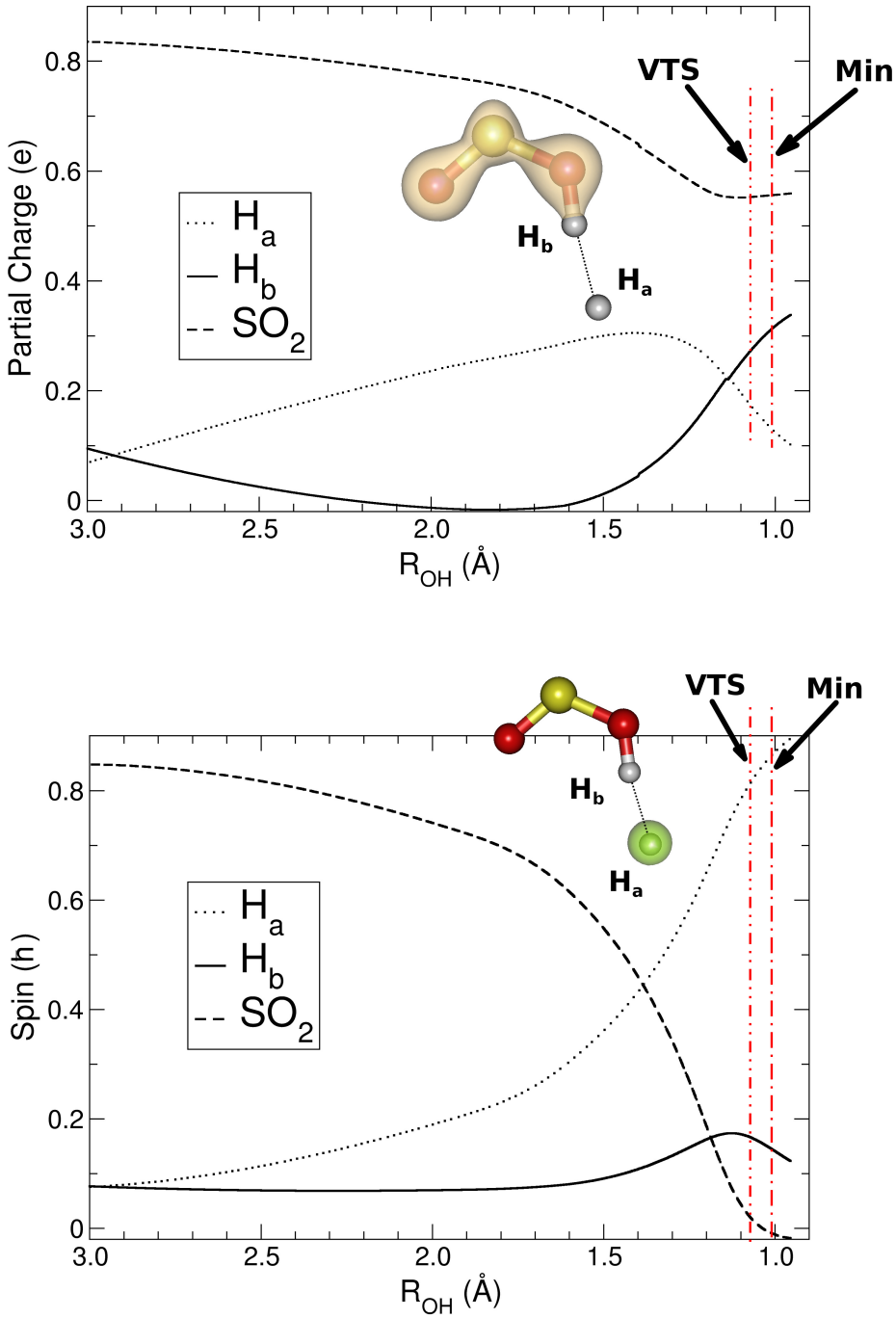

Figure 5: Mulliken Atomic Charge (Top panel) and Spin population (Bottom panel) along the MEP in the region of the reaction. See further details in the main text.

the **VTS** structure comes before the **Min** adduct in the reaction coordinate (Figure 4), and the dynamical evolution of the charge and spin distribution (Figure 5) in the complex along the reaction path is very different from that of the reaction of SO_2^+ with water[33]. As

for the partial charges and spin in the reaction complex $[O_dSO_c \cdots H_bH_a]^+$ in the region of approaching reagents, the charge and the spin remain mainly localized on SO_2^+. Moving forward with the reaction up to $R_{OH} = 1.5$ Å the charge increases on H_a from 0.0 to + 0.3 e and decreases on SO_2^+ from 1.0 to 0.7 e and on H_b from 0.1 to 0.0 e (see top panel of Figure 5). The spin remains almost constant on H_b, but it decreases for SO_2^+ from 1.0 to 0.5$\hbar$, and increases for H_a from 0.0 to 0.4$\hbar$ (see bottom panel of Figure 5). On the other hand, in the region of the **Min** the charge decreases on H_a and increase on H_b, while the spin goes to zero for SO_2^+, and increases for H_a up to 1.0 $\hbar$. It is interesting to note that, in the reaction of SO_2^+ with water, the chemical rearrangement occurs at the beginning of the reaction with a fast proton-coupled electron transfer[33]. The higher IE 15.4 eV of H_2 relative to IE 12.6 eV of H_2O, the lowest H_2 polarizability (see Table 1) and the higher relative stability of OH (ΔH_f^o= +38.99 kJ/mol) with respect to H (ΔH_f^o= +218.0 kJ/mol) make the reaction dynamics of $SO_2^+ + H_2$ more constrained and slower[47]. The "bottleneck" of the reaction's trajectories, occurring at the **VTS** complex, reduces the reactivity below the collision limit of $1.53 \cdot 10^{-9}$ cm^{3}molecule^{-1}s^{-1}.

Theoretical rate coefficients. The VTST allows the calculation of the kinetic coefficients (k) trough the following equation (see theoretical section for more details):

$$k(T) = \sigma \frac{k_B T}{h} exp\left[\frac{Q_{\mathbf{VTS}}(T)}{Q_{SO_2^+}(T) Q_{H_2}(T)}\right] \tag{3}$$

which holds in thermal equilibrium conditions (Canonical ensemble). In eq 3 σ is the symmetry factor, $Q_{\mathbf{VTS}}(T)$ is the total molecular partition function of the reaction complex divided for the $Q_{vib}^{irc}(T)$, the molecular vibrational partition function of the frequency associated to the internal reaction coordinate (irc) over which the MEP is computed. $Q_{SO_2^+}(T)$ and $Q_{H_2}(T)$ are the total molecular partition functions of the reactants - each can be factorized in the usual electronic, vibrational, rotational and translational factors: $Q(T) = Q_{el}(T)Q_{vib}(T)Q_{rot}(T)Q_{tr}(T)$.

A value of $2.9 \cdot 10^{-11}$ cm^{3}molecule^{-1}s^{-1} was obtained at 300 K by eq 3 for reaction

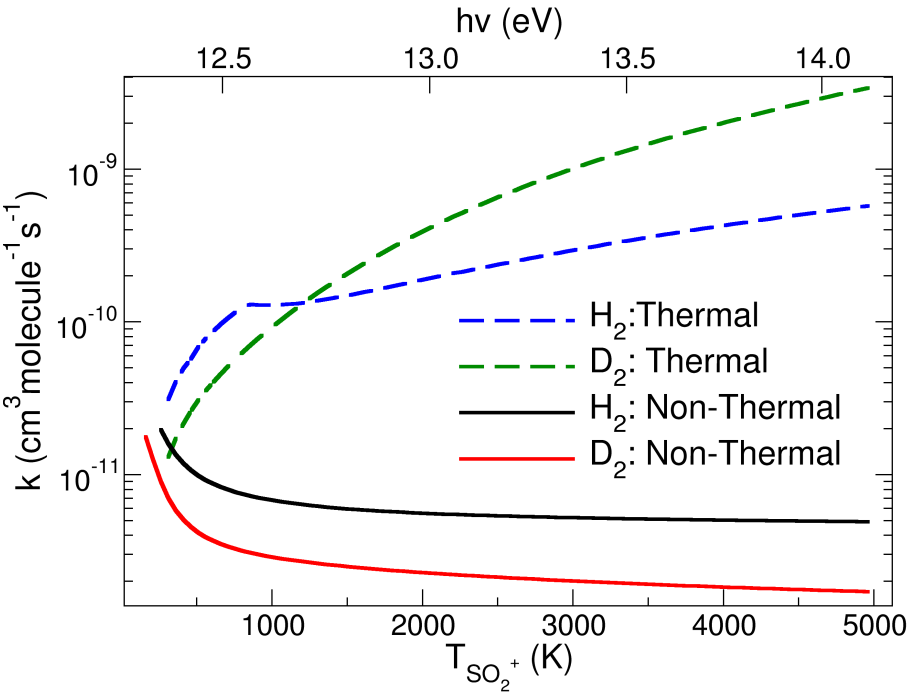

Figure 6: Rate coefficients for the reactions of SO_2^+ with H_2 and D_2 calculated both under thermal equilibrium conditions and with the non-thermal model. See further details in the main text.

$SO_2^+ + H_2$, close to that obtained experimentally by Anicich[49]. The calculated k for the reaction with D_2 is $1.51 \cdot 10^{-11}$ cm^3 molecule^{-1}s^{-1}, smaller than that with H_2, and with an isotope effect of 1.92 at 300 K. The rate coefficient k for the reaction with H_2 calculated from eq 3, increases monotonically with the temperature as shown by the blue dashed line in Figure 6. The same trend is observed for the reaction with D_2 (green dashed line of Figure 6). The thermal rate for H_2 changes its slope at about 800 K, while this is not the case for D_2. This different trend with temperature leads to the crossing of the two rates at about 1200 K, where the rate coefficient of D_2 becomes higher than the rate of H_2. This behavior is due to the different increase of the $Q(T)$ of H_2 relative to that of D_2 caused by a different population with temperature of the respective calculated vibrational levels: $\nu^{H_2}_{stretching} = 4381$ cm^{-1}, $\nu^{D_2}_{stretching} = 3100$ cm^{-1}.

It is proper to point out here that the experimental data are acquired as a function of the photon energy which simultaneously ionize the neutral and excite the ro-vibration levels of the ion, meanwhile the calculated rate coefficient (eq 3) is a function of the temperature. In order to have the rate coefficient as a function of the photon energy, we proceed as follow. A complete conversion of electronic excitation of the ion into ro-vibrational excitation by internal relaxation[33] is assumed, and an internal temperature for SO_2^+ is defined with a dependence from the ro-vibrational excitation energy $E^{int}_{SO_2^+}$:

$$E^{int}_{SO_2^+} = 3/2 K_B T_{SO_2^+} + E^{vib}_{exc}(T_{SO_2^+}) \tag{4}$$

where the first term is the thermal rotational energy for a non-linear molecule, and the second term is the vibrational excitation energy[55]:

$$E^{vib}_{exc}(T_{SO_2^+}) = \sum_{i=1}^{3N-6} \frac{h\nu_i}{e^{h\nu_i/k_B T_{SO_2^+}} - 1} \tag{5}$$

where ν_i is the ith vibrational frequency of the ion. Hence, in the top axis of abscissas of Figure 6 we have reported the photon energy ($h\nu = IE(SO_2) + E^{int}_{SO_2^+}$), while on the bottom axis of abscissas it is reported the temperature of the excited ion. It is evident that the trend of the thermal rates (blue and green lines of Figure 6) does not match the experimental observation, where a decrease of the ratio ($H(D)SO_2^+/SO_2^+$) is recorded with the increase of internal energy of SO_2^+ when the photon energy is greater then 12.4 eV (Figure 3). The mismatch between the experimental product/reactant ratio and the theoretical thermal rates led us to carefully analyze the compliance of the experimental conditions with the hypotheses underneath the VTS model. In particular we observe that:

1. The SO_2^+ ion has an internal energy content given by the absorption of the VUV photon, ranging from room temperature, when the incident photon is at the ionization threshold, up to several thousands of Kelvin degrees. On the other hand, the H_2 neutral reactant has an energy content given by its thermal state, which corresponds

to the room temperature at which the experiment is performed. Due to low pressure conditions, the thermalization by collisions between the "heated up" ion SO_2^+ and the neutral H_2 can be neglected in the timescale of measurements.

2. The reactive complex formed by SO_2^+ and H_2, whose geometric parameters at the minimum energy are reported in Table 2, is not in thermal equilibrium with the other molecules present in the reaction chamber (low pressure conditions), and in addition it is characterized by non-thermal equilibrium within its internal vibrational degrees of freedom. On the one hand, the energy redistribution within the **VTS** complex, which moves downhill along the MEP, is such that the released potential energy (85 kJ/mol) is preferentially localized over the reaction coordinate $H-H$ due to the fact that the **VTS** complex is in the product region. On the other hand, the energy transferred by the absorption of the VUV radiation is mainly localized in the HSO_2 part of the **VTS** complex.

Since the IVR (Internal Vibrational Redistribution) within the **VTS** complex can be considered slower then the fast barrierless reaction, we can reasonably assume that the **VTS** complex is non-ergodic in the present experimental conditions[56]. The energy flux within the **VTS** complex is controlled by the IVR processes occurring between the reaction coordinate stretching $H-H$ and the internal degrees of freedom of HSO_2. We hypothesize that during the reaction the energy flux is from the HSO_2 subset of the **VTS** complex towards the reaction coordinate $H-H$, with an increase of the energy flux as the energy content of SO_2^+ increases. The reasons beyond this assumptions are due to the fact that the IVR rate is: *i*) proportional to the density of the final states, and *ii*) is inversely proportional to the exponential of the energy difference between the initial and final states of the IVR (see eq. 5-2 of reference[57]). Hence, as the SO_2^+ is excited, the **VTS** complex reaches higher energy states which efficiently couple with the high energy states of the reaction coordinate $H-H$, populated during the downhill along the MEP.

The VTST approach, which assumes a local-equilibrium, namely a fast and full molecular

energy redistribution in the reaction system, is generally valid when the reactants couple their degrees of freedom within the reactive complex. If the reaction follows a statistic energy redistribution, faster than reaction time, a local thermal equilibrium is always reached [58,59]. The hydrogen molecule, which has a very high vibrational stretching frequency due to its light mass, is an optimal neutral reagent to check how much IVR is efficient; i.e. if its high energy vibration can efficiently couple with the other vibrations within the complex. It is known that the VTST is generally valid, but it could fail when a high frequency vibration does not couple efficiently to other low frequencies in a reaction complex as, for instance, in the case of the reaction of H with OH leading to a non-equilibrium effects [60–62].

Following the hypothesis discussed above, we have reformulated the model to calculate the rate coefficient. Eq 3 has been therefore adapted to the conditions of the experiments. We assume that the molecular partition function of H_2 is fixed at 300 K, the partition function of the **VTS** is factorized in two terms: an effective temperature dependent ro-vibrational part $Q_{VTS}^{ro-vib(SO_2^+)}(T_{eff})$ and a translational factor constant with temperature $Q_{VTS}^{tr}(300K)$. The effective temperature (T_{eff}) is a function of the temperature of SO_2^+, and takes into account the part of the ro-vibrational energy which is transferred to the $H-H$ coordinate during the reaction . Eq 3 is modified according to the above consideration, and the non-thermal rate coefficient k^{NT} becomes:

$$k^{NT}(T_{SO_2^+}) = \sigma \frac{k_B 300K}{h} exp\left[\frac{Q_{VTS}^{ro-vib}(T_{eff})Q_{VTS}^{tr}(300K)}{Q_{SO_2^+}(T_{SO_2^+})Q_{H_2}(300K)}\right] \tag{6}$$

We have parameterized the effective temperature in order to reproduce the experimental trend of the data in Figure 3:

$$T_{eff}(T_{SO_2^+}) = \alpha + \beta T_{SO_2^+}^{\gamma} - \frac{\delta}{T_{SO_2^+}} \tag{7}$$

The parameters used are reported in Table 3, while in Figure S2 of SI the $T_{eff}(T_{SO_2^+})$ for both H_2 and D_2 are reported.

Table 3: Parameters for the T_{eff} dependence from $T_{SO_2^+}$: α is in K, β is in $K^{1-\gamma}$, γ and δ are dimensionless.

	α	β	γ	δ
H_2	129.577	0.642	1.013	11273.0
D_2	197.510	7.221	0.493	10821.7

The non-thermal conditions produce an energy flow in the **VTS** complex which can be analyzed in term of the energy in the reaction coordinate $H - H$ and in all the other ro-vibrational degrees of freedom, whose vibrational frequencies are reported in Figure S3 and S4 of SI. In Figure 7 the internal energy of the **VTS** complex E^{int}_{VTS} (See eq 1 of SI), and of the reaction coordinate E^{int}_{RC} (See eq 3 of SI) for both the reaction with H_2 and D_2 are reported as a function of the temperature $T_{SO_2^+}$, and its associated energy $E^{int}_{SO_2^+}$, which is also reported in the same figure. The energy is clearly preferentially stored in the reaction coordinate, especially when the $T_{SO_2^+}$ increases. This can be rationalized in term of the IVR rate, which is more efficient when transferring energy from the **VTS** complex to the reaction coordinate then vice-versa. This is also in agreement with the experimental product/reagent ratio, which decreases as the energy of the SO_2^+ increases. This counter-intuitive trend can be explained considering that the excitation photon energy acquired by the **VTS** complex is not used to increase the number of trajectories in the phase space of the reaction which leads to the products, but this excitation energy is almost entirely directed into the reaction coordinate, which at the end of the reaction will determine a high kinetic energy content of the H/D atom product.

By plotting the rate coefficient of eq 6 as a function of the temperature (see black line of Figure 6), it is evident that the behavior of the rate coefficient for reaction with H_2 is completely different from that obtained with thermal equilibrium conditions using eq 3, (blue line in Figure 6). The thermal approach produces an increase of the rate coefficient with temperature, whereas the non-thermal rate exhibits a decrease with temperature. We cannot make a quantitative comparison between the new theoretical $k^{NT}(T_{eff})$ and the experimental ion yield, but certainly the very interesting result is that the trend (black line of Figure 6) is

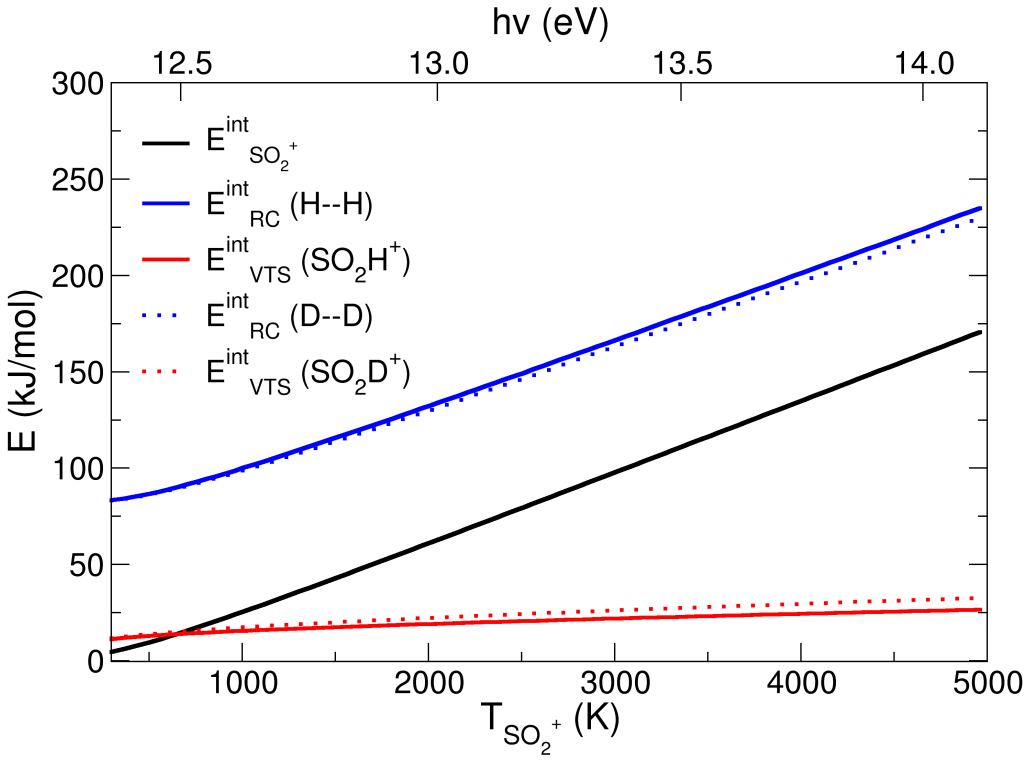

Figure 7: Energy redistribution for the reactions of SO_2^+ with H_2 and D_2 calculated as a function of the temperature of the ionic reagent. See further details in the main text.

consistent with the experimental one (black line in Figure 3). The same considerations are valid for the reaction with D_2. Moreover, at 300 K, when all the vibrational modes are at the same temperature, a value of $1.66 \cdot 10^{-11}$ cm^{3}molecule^{-1}s^{-1} is calculated for $SO_2^+ + H_2$ reaction, in agreement with the experimental rate constant $1.7{\cdot}10^{-11}{\pm}40\%$ cm^{3}molecule^{-1}s^{-1} [49]. It is noteworthy to mention that the same discrepancy between experiments and theory was also observed in the reaction of CH_4^+ with H_2 at temperatures higher then 100 K[26,27,63]. In table S1 of SI the parameters of the fitting of the rate coefficients for reactions of SO_2^+ with H_2O, CH_4, H_2 and D_2 in the temperature range 300-5000 K are reported.

***SO_2^+* reactivity in the *O_3* depletion and *OH* formation**. The potential relevance in the stratospheric environment of the reactions involving SO_2^+ with neutral species such as H_2O, CH_4 and H_2 is strictly connected with their fast rate coefficients leading to HSO_2^+ and

relevant radical species such as OH, CH_3 and H. The hydrogen atom quickly reacts with O_3 producing O_2 and OH (see eq 2), with the effect of destroying O_3 and increasing the amount of hydroxyl radical. This is the most important oxidant in the stratosphere[34], which oxides the SO_2 to HSO_3, triggering the process which leads to H_2SO_4 aerosol formation[14,64]. The main source of OH during daytime is the reactions of water (eq 9) and molecular hydrogen (eq 10) with $O(^1D)$[14], produced by sunlight photodissociation of ozone (eq 8), while OH density is strongly reduced during nighttime[65]:

$$O_3 + h\nu \rightarrow O_2 + O(^1D) \tag{8}$$

$$O(^1D) + H_2O \rightarrow 2OH \tag{9}$$

$$O(^1D) + H_2 \rightarrow OH + H \tag{10}$$

On the basis of the chemical reactions eqs 8-10 the oxidation of SO_2 should only occur in the daytime, whereas clear evidences[66] exist that a significant amount of SO_2 is oxidized during the night. Indeed, alternative oxidation pathways leading to sulfuric acid have been investigated, and ionic mechanisms seem to be operative during the night due to ionizing radiation[18]. Hence, the OH produced by the reactions of SO_2^+ with water[33] ($SO_2^+ + H_2O \rightarrow HSO_2^+ + OH$) and H_2 (trough eq 2) should be considered as potential relevant ionic processes of H_2SO_4 aerosol formation during nighttime, and should be tested in the atmospheric models.

Common rate coefficients of ion-molecule reactions involving SO_2^+ ($10^{-11} - 10^{-9}$ cm^3 molecule^{-1} s^{-1}) are several orders of magnitude higher than the rate coefficient of the oxidation of SO_2 by OH, which in standard stratospheric pressure and temperature conditions can be reduced to a pseudo second order reaction, with a rate coefficient[64] of about $5 \cdot 10^{-16}$ cm^{3}molecule^{-1}s^{-1} . Obviously, the relative efficiency of these neutral-neutral and ion-neutral

reactions does not only depend on the relative rate coefficients, but also on the relative concentration of the reagents. These concentrations change with the the altitude for H_2O, CH_4 and H_2, as well as with the day-time cycle for the OH[65]; whereas the relative abundance of SO_2^+/SO_2 ($\sim 10^{-12}$) is almost constant[19]. Solar geoengineering schemes require that SO_2 is at a pressure of 1 bar when injected by balloons or aircrafts[67], this implies that the SO_2^+ density could locally reach a maximum value of about 10^7 ions/cm^3, which is a relevant concentration for the chemistry in the stratosphere. On the basis of the discussion above, the ion-neutral reactions involving SO_2^+ and leading to OH may be considered as a relevant source of OH which can oxide SO_2 during the night, when OH can not be produced via neutral-neutral reactions triggered by sunlight. The alternative routes for the oxidation of SO_2^+ and HSO_2^+ by O_3 have been also considered in the present study:

$$SO_2^+ + O_3 \rightarrow SO_3^+ + O_2(^1\Delta_g) \tag{11}$$

$$HSO_2^+ + O_3 \rightarrow HSO_3^+ + O_2(^1\Delta_g) \tag{12}$$

Both reactions in eqs. 11 and 12 are exothermic by 102.9 and 93.4 kJ/mol, respectively[47,48]. The rate coefficients for these reactions have not been so far determined, hence their MEP have been calculated in this work (see Figure S5 of SI). Both reactions result to be barrierless, with VTS calculated rate coefficients at 300 K of $3 \cdot 10^{-17}$ cm^{3}molecule^{-1}s^{-1} (eq 11), and $8 \cdot 10^{-15}$ cm^{3}molecule^{-1}s^{-1} (eq 12). These rate coefficients indicate that these oxidation reactions are negligible with respect to oxidation of SO_2 by OH produced by reaction of SO_2^+ with water and molecular hydrogen during nighttime.

It is also noteworthy to say that HSO_2^+ fast reacts[30,33] with water leading to H_3O^+ and SO_2. The latter, once re-ionized, can act as a catalyst in the formation of hydronium ion, a dominant ionic species in the stratosphere[68].

Conclusions

In this work the reaction of the radical cation SO_2^+ with H_2/D_2 has been explored at low pressures, mainly focusing on non thermal effects in the redistribution of the internal energy within the reactive complex. The reaction is a barrierless exothermic process, guided by a molecular complex whose substantial charge and spin changes along the reaction coordinate are the factors that slow down the reactivity of the system. The experimental results show that the ratio $H(D)SO_2^+/SO_2^+$ decreases when the SO_2^+ ion is excited in the ro-vibrational levels of its ground electronic state. DFT and VTST theories have been used to study the dynamic of the reaction along the MEP, where a **VTS** reaction complex $[OSOH\cdots H]^+$ has been identified as the "bottleneck" which controls the reactivity of the system. Standard VTST allows the calculation of the rate coefficient at different excitation energy of SO_2^+. The value at 300 K is $2.9\cdot10^{-11}$ cm^{3}molecule^{-1}s^{-1} in reasonable agreement with the value of $1.7\cdot10^{-11}\pm40\%$ cm^{3}molecule^{-1}s^{-1} measured with a ICR instrument. At higher excitation energy of SO_2^+ the standard VTST rate coefficient k increases within the frame of the thermal equilibrium model, while a decrease of the ratio $H(D)SO_2^+/SO_2^+$ is observed in the experiments. This opposite trend between theory and experiment has been attributed to a fast reaction dynamics with the light hydrogen atoms, where the thermal equilibrium approximation holds no more. This favors the IVR processes which transfer ro-vibrational energy from the **VTS** reaction complex towards the reaction coordinate $H-H$.

The non-thermal assumptions have been taken into account in the calculation of partition functions of H_2 and **VTS**. The H_2 temperature has been kept at 300 K, the temperature in the experimental apparatus, while the **VTS** has been evaluated at an effective temperature parameterized over the experimental product/reagent ratio. The rate coefficients obtained with this non-thermal model decrease with the increase of the excitation energy of SO_2^+, consistently with the experimental data.

The ionization of SO_2 and its reactions with neutral molecules such as H_2 and H_2O in the stratosphere should be considered as relevant channels in the OH production during

nighttime, when the common neutral-neutral reactions producing OH via sunlight are not at work. Hence, in the night the above ion-neutral reactions may trigger the oxidation of SO_2, which subsequently leads to H_2SO_4 aerosol formation. This may explain the decrease of SO_2 observed during the nighttime by several studies. Moreover, the reaction of SO_2^+ with H_2 is relevant for the ozone depletion process. The results of this work indicate that the SO_2^+ ion chemistry should be considered and tested in the atmospheric models for solar geoengineering strategies in the stratosphere.

Experimental Section

The description of the CiPo beamline at ELETTRA has been reported previously[32,69–73]. Briefly, the beamline is equipped with an electromagnetic elliptical undulator/wiggler and a Normal Incidence Monochromator (NIM) to cover the vacuum ultraviolet (VUV) 8-40 eV energy range. The aluminum grating of the NIM operates in the energy range 8-17 eV with a resolving power of about 1000. The photon energy was calibrated against the autoionization features observed in the Ar total photoionization between the 3p spin orbit components[74]. The SO_2 is introduced in the ionization source at the pressure of about $5.0 \cdot 10^{-6}$ mbar and ionized with the VUV radiation. The ions produced at a photon energy higher than the ionization threshold (about 12.4 eV) are internally excited. The SO_2^+ ions are guided into the octupole (reactive zone) at a CE=0.0 eV, which is determined by measuring the SO_2^+ yield as a function of the retarding field. The estimated energy spread is about 100 meV. The neutral reagent H_2/D_2 gas is introduced in the reactive zone by a needle valve at pressure of about 10^{-5} mbar and room temperature. The ion-molecule reaction of SO_2^+ with H_2/D_2 is followed by recording the yields of ionic reagent (m/z 64) and ionic product (m/z 65 or 66), corrected for the natural isotopic abundance[47] contribution of ^{33}S, ^{17}O, ^{34}S, ^{18}O, as a function of the photon energy from 12.4 to 15.0 eV in steps of 100 meV and with the acquisition time of 30 s/point. The pressure and CE were kept fixed during the energy scan. The mass spectrum of all the ionic species has been acquired in the mass over charge

range 10<m/z<70 (acquisition time of 3 s/point) at the photon energy $h\nu$=14.0 eV, and CE=0.0 eV. The presence of possible contaminants in the apparatus, as water, has been checked and excluded with and without the neutral (H_2/D_2) inside the octupole. Sometime a small amount of SO^+ due to the ionization of SO_2, without the neutral in the reaction zone, has been observed. However, it is well known the SO^+ does not affect the title reaction since it does no react with H_2 as also verified in our experiments[49]. The reaction efficiencies were evaluated by calculating the ratio HSO_2^+/SO_2^+ and using statistical propagation error formula to estimate the error bars. Data analysis has been performed using OriginPro8 program.

Materials. All the samples were used at room temperature. Sulfur dioxide was purchased from Sigma-Aldrich with a purity > 99.98% whereas hydrogen H_2 and deuterium D_2 are from SIAD with purity > 99.99%.

Theoretical Section

The energetic and dynamical description of the title reaction has been based on the Density Functional Theory formalism, which has been used to explore the Potential Energy landscape of the hydrogen transfer from H_2 to the SO_2^+ ion. The hybrid exchange-correlation functional Becke, three-parameter, Lee-Yang-Parr[75–78] has been used with the split-valence double-zeta Pople with polarization and diffuse functions: 6-31++g** basis set[79,80]. The region of reaction of the PES has been computed by full optimizations by scanning the R_{O-H} and R_{H-H} coordinates, where the hydrogen atom is involved in the exchange with the O atom of the SO_2 ion. The scanning coordinate R_{O-H} started at a 0.9 Å and ended at 4.0 Å, the coordinate R_{H-H} was scanned by starting at 0.77 Å up to 5.0 Å, both coordinates were scanned with a variable step whose minimum value as been taken as 0.00375 Å: this quantum calculation has generated a Minimum Energy Path (MEP) which is needed to compute the reaction rate coefficients. The variational transition state theory (VTST) model, specifically developed for applications with barrierless reactions[60] has been adopted here to model the

present reaction. All these calculations have been corrected by the zero point energies, with the underlying harmonic vibrational frequencies scaled by the coefficient 0.986 [81]. The charge and spin population are based on the Mulliken analysis of the electron density [82]. The MEP has been used to compute the total molecular partition functions [Q(T)] of the reactive complex $[OSO \cdots H_2]^+$ in the range of temperatures 300-2000K. Within the Variational Transition State Theory (VTST) [40] these partition functions are used to localize the kinetic bottleneck of the reactive flux of trajectories moving along the MEP. The reactions 11 and 12 have been studied with a lower level of accuracy, in particular the O-O coordinate has been scanned with a fixed step of 0.05 Å, which could overestimate the VTS rate coefficients. A smaller step in the scanning of the MEP has not been performed since these rate coefficients are already too low to be considered in reactive chemical network of atmospheric models. All the quantum chemical calculations were performed with the Gaussian09 package [83].

Acknowledgments

The work has been supported by the MIUR FIRB RBFR10SQZI project. The authors thank Fabio Zuccaro for his excellent technical assistance.

References

(1) *Climate Intervention: Reflecting Sunlight to Cool Earth*; Washington, DC: THE NATIONAL ACADEMIES PRESS, 2015; https://doi.org/10.17226/18988.

(2) Caldeira, K.; Bala, G.; Cao, L. The science of geoengineering. *Annu. Rev. of Earth and Pl. Sci.* **2013**, *41*, 231–256.

(3) Marchetti, C. On geoengineering and the CO_2 problem. *Clim. Change* **1977**, *1*, 59–68.

(4) Keith, D. W. Geoengineering the climate: History and prospect. *Annu. Rev. Energ. Environ.* **2000**, *25*, 245–284.

(5) Robock, A.; Oman, L.; Stenchikov, G. L. Regional climate responses to geoengineering with tropical and Arctic SO_2 injections. *J.Geophys. Res.* **2008**, *113*, D16101.

(6) Irvine, P.; Emanuel, K.; He, J.; Horowitz, L. W.; Vecchi, G.; Keith, D. Halving warming with idealized solar geoengineering moderates key climate hazards. *Nat. Clim. Change* **2019**, *9*, 295–299.

(7) Heckendorn, P.; Weisenstein, D.; Fueglistaler, S.; Luo, B. P.; Rozanov, E.; Schraner, M.; Thomason, L. W.; Peter, T. The impact of geoengineering aerosols on stratospheric temperature and ozone. *Environ. Res. Lett.* **2009**, *4*, 045108.

(8) Crutzen, P. J. Albedo enhancement by stratospheric sulfur injections: A contribution to resolve a policy dilemma? *Clim. Change* **2006**, *77*, 211–219.

(9) Niemeier, U.; Tilmes, S. Sulfur injections for a cooler planet. *Science* **2017**, *357*, 246.

(10) Tollefson, J. Geoengineering debate shifts to un environment assembly. *Nature* **2019**, *567*, 156.

(11) Lawrence, M. G.; Schafer, S.; Muri, H.; Scott, V.; Oschlies, N. E., A. Vaughan; Boucher, H., O. Schmidt; Haywood, J.; Scheffran, J. Evaluating climate geoengineering proposals in the context of the Paris Agreement temperature goals. *Nat. Comm.* **2018**, *9*, 3734.

(12) Jones, . C.; Haywood, J. M.; Dunstone, N.; Emanuel, K.; Hawcroft, M. K.; Hodges, K. I.; Jones, A. Impacts of hemispheric solar geoengineering on tropical cyclone frequency. *Nat. Comm.* **2017**, *8*, 1382.

(13) Trisos, C. H.; Amatulli, G.; Gurevitch, J.; Robock, A.; Xia, L.; Zambri, B. Potentially dangerous consequences for biodiversity of solar geoengineering implementation and termination. *Nat. Ecol. & Evol.* **2018**, *2*, 475–482.

(14) Burkholder, J. B.; Sander, S. P.; Abbatt, J. R., J. amd Barker; Huie, R. E.; Kolb, C. E.; Kurylo, M. J.; Orkin, V. L.; Wilmouth, D. M.; ; Wine, P. H. *Chemical Kinetics and Photochemical Data for Use in Atmospheric Studies, Evaluation No. 18,*; 2015; JPL Publication 15-10, http://jpldataeval.jpl.nasa.gov.

(15) Aplin, K. L.; Briggs, A. A.; Harrison, R. G.; Marlton, G. J. Measuring ionizing radiation in the atmosphere with a new balloon-borne detector. *Space Weather* **2017**, *15*, 663–672.

(16) Bazilevskaya, G. A.; Usoskin, I. G.; Fluckiger, E. O.; Harrison, R. G.; Â· Desorgher, L.; Butikofer, R.; Krainev, M. B.; Makhmutov, V. S.; Stozhkov, Y. I.; Svirzhevskaya, A. K.; Svirzhevsky, N. S.; Kovaltsov, G. A. Cosmic Ray Induced Ion Production in the Atmosphere. *Space Sci. Rev.* **2008**, *137*, 149–173.

(17) Stozhkov, Y. I.; Svirzhevsky, N. S.; Bazilevskaya, G. A.; Kvashnin, A. N.; Makhmutov, V. S.; Svirzhevskaya, A. K. Long-term (50 years) measurements of cosmic ray fluxes in the atmosphere. *Adv. Space Res.* **2009**, *44*, 124–1137.

(18) Enghoff, M. B.; Bork, N.; Hattori, S.; Meusinger, C.; Nakagawa, M.; Pedersen, J. O. P.; Danielache, S.; Ueno, Y.; Johnson, M. S.; Yoshida, N.; Svensmark, H. An isotopic analysis of ionising radiation as a source of sulphuric acid. *Atmospheric Chemistry and Physics* **2012**, *12*, 5319–5327.

(19) Shuman, N. S.; Hunton, D. E.; Viggiano, A. A. Ambient and Modified Atmospheric Ion Chemistry: From Top to Bottom. *Chemical Reviews* **2015**, *115*, 4542–4570.

(20) Svensmark, H.; Enghoff, M. B.; Shaviv, N. J.; Svensmark, J. Increased ionization supports growth of aerosols into cloud condensation nuclei. *Nat. Comm.* **2017**, *8*, 2199.

(21) Dai, Z.; Weisenstein, D. K.; Keith, D. W. Tailoring Meridional and Seasonal Radiative Forcing by Sulfate Aerosol Solar Geoengineering. *Geophys. Res. Lett.* **2018**, *45*, 1030.

(22) Kharchenko, V.; Dalgarno, A. Thermalization of fast O(1D) atoms in the stratosphere and mesosphere. *J. Geophys. Res.* **2004**, *109*, D18311.

(23) Takahashi, K.; Taniguchi, N.; Sato, Y.; Matsumi, Y. Nonthermal steady state translational energy distributions of O(1D) atoms in the stratosphere. *J. Geophys. Res.* **2002**, *107*, 4290.

(24) Wise, J. O.; Smith, D. R.; Wheeler, N. B.; Ahmadjian, M.; Nadile, R. M. Overview and Summary of Results and Signicant Findings from the CIRRIS-1A Experiment. *J. Spacecr. Rockets* **2001**, *38*, 297.

(25) Goss-Custard, M.; Remedios, J. J.; Lambert, A.; Taylor, E. W.; Rodgers, C. D.; Lopez-Puertas, M.; Zaragoza, G.; Gunson, M. R.; Suttie, M. R.; Harries, J. E.; Russell, J. M. Measurements of water vapor distributions by the improved stratospheric and mesospheric sounder: Retrieval and validation. *J. Geophys. Res.* **1996**, *101*, 9907.

(26) Asvany, O.; Savic, I.; Schlemmer, S.; Gerlich, D. Variable temperature ion trap studies of $CH_4 + H_2$, HD and D_2:negative temperature dependence and significant isotope effect. *Chem.Phys.* **2004**, *298*, 97–105.

(27) Wang, B.; Hou, H. Computational Study of the Ion-Molecule Reactions Involving Fluxional Cations: $CH_4^+ + H_2 \rightarrow CH_5^+ + H$ and Isotope Effect. *J. Phys. Chem. A* **2005**, *109*, 8537–8547.

(28) Rockmann, T.; Rhee, T. S.; Engel, A. Heavy hydrogen in the stratosphere. *Atmos. Chem. Phys. Discuss.* **2003**, *3*, 3745–3768.

(29) de Petris, G.; Cartoni, A.; Troiani, A.; Barone, V.; Cimino, P.; Angelini, G.; Ursini, O. Double C-H Activation of Ethane by Metal-Free SO_2^+ Radical Cations. *Chem. Eur. J.* **2010**, *16*, 6234–6242.

(30) de Petris, G.; Cartoni, A.; Troiani, A.; Angelini, G.; Ursini, O. Water activation by SO_2^+ ions: an effective source of OH radicals. *Phys. Chem. Chem. Phys.* **2009**, *11*, 9976–9978.

(31) de Petris, G.; Cartoni, A.; Rosi, M.; Barone, V.; Puzzarini, C.; Troiani, A. The Proton Affinity and Gas-Phase Basicity of Sulfur Dioxide. *ChemPhysChem* **2011**, *12*, 112–115.

(32) Catone, D.; Satta, M.; Cartoni, A.; Castrovilli, M. C.; Bolognesi, P.; Avaldi, L. Electrophilic Gas Phase Oxidation of Carbon Monoxide by Sulfur Dioxide Radical Cation: Reaction Dynamic and Kinetic Trend with the Temperature. *Front. Chem.* **2019**, *7*, 1–10.

(33) Cartoni, A.; Catone, D.; Bolognesi, P.; Satta, M.; Markus, P.; Avaldi, L. HSO_2^+ Formation from Ion-Molecule Reactions of SO_2^+ with Water and Methane: Two Fast Reactions with Reverse Temperature-Dependent Kinetic Trend. *Chem. Eur. J.* **2017**, *23*, 6772–6780.

(34) Martins-Costa, M. T. C.; Anglada, J. M.; Francisco, J. S.; Ruiz-Lopez, M. F. Photochemistry of SO_2 at the Air-Water Interface: A Source of OH and HOSO Radicals. *J. Am. Chem. Soc.* **2018**, *140*, 12341–12344.

(35) Ruiz-Lopez, M. F.; Martins-Costa, M. T. C.; Anglada, J. M.; Francisco, J. S. A New Mechanism of Acid Rain Generation from HOSO at the Air-Water Interface. *J. Am. Chem. Soc.* **2019**,

(36) Murphy, D. M.; Thomson, D. S.; Mahoney, M. J. In Situ Measurements of Organics, Meteoritic Material, Mercury, and Other Elements in Aerosols at 5 to 19 Kilometers. *Science* **1998**, *282*, 1664–1669.

(37) Vereecken, L.; Francisco, J. S. Theoretical studies of atmospheric reaction mechanisms in the troposphere. *Chem. Soc. Rev.* **2012**, *41*, 6259–6293.

(38) Long, B.; Bao, J. L.; Truhlar, D. G. Atmospheric Chemistry of Criegee Intermediates: Unimolecular Reactions and Reactions with Water. *J. Am. Chem. Soc.* **2016**, *138*.

(39) Truhlar, D. G.; Garrett, B. C. Variational Transition State Theory. *Annu. Rev. Phys. Chem.* **1984**, *35*, 159–189.

(40) Bao, J. L.; Truhlar, D. G. Variational transition state theory: theoretical framework and recent developments. *Chem. Soc. Rev.* **2017**, *46*, 7548–7596.

(41) Fairley, D.; Scott, G.; Milligan, D.; Maclagan, R.; McEwan, M. SIFDT study of the SO_2^+/H_2 H-atom abstraction reaction. *Int. J. Mass Spectrom.* **1998**, *172*, 79–87.

(42) Scott, G. B.; Fairley, D. A.; Freeman, C. G.; McEwan, M. J.; Spanel, P.; Smith, D. Gas phase reactions of some positive ions with atomic and molecular hydrogen at 300 K. *J. Chem. Phys.* **1997**, *106*, 3982.

(43) Derossi, A.; Lama, F.; Piacentini, M.; Prosperi, T.; Zema, N. High flux and high resolution beamline for elliptically polarized radiation in the vacuum ultraviolet and soft x-ray regions. *Rev. Sci. Instrum.* **1995**, *66*, 1718–1720.

(44) Li, W. Z.; Huang, M. B.; Chen, B. Z. The 1^2A_1 , 1^2B_2 , and 1^2A_2 states of the SO_2^+ ion studied using multiconfiguration second-order perturbation theory. *J. Chem. Phys.* **2004**, *120*, 4677–4682.

(45) Holland, D. M. P.; MacDonald, M. A.; Hayes, M. A.; Baltzer, P.; Karlsson, L.; Lundqvist, M.; Wannberg, B.; von Niessen, W. An experimental and theoretical study of the valence shell photoelectron spectrum of sulphur dioxide. *Chem. Phys.* **1994**, *188*, 317–337.

(46) Brehm, B.; Eland, J.; Frey, R.; Kustler, A. Predissociation ofSO_2^+ ions studied by photoelectron-photoion coincidence spectroscopy. *Int. J. Mass Spectrom. Ion Phys.* **1973**, *12*, 197–211.

(47) *Computational Chemistry Comparison and Benchmark Database NIST Standard Reference Database Number 101 Release 19*; April 2018.

(48) Lias, S.; Bartmess, J.; Liebman, J.; Holmes, J.; Levin, R.; Mallard, W. Gas-phase ion and neutral thermchemistry. *J. Phys. Ref. Data* **1988**, *17*, Suppl. No.1.

(49) Anicich, V. G. Evaluated Bimolecular Ion-Molecule Gas Phase Kinetics of Positive Ions for Use in Modeling Planetary Atmospheres, Cometary Comae, and Interstellar Clouds. *J. Phys.Chem. Ref. Data* **1993**, *22*, 1469–1569.

(50) Su, T.; Chesnavich, W. J. Parametrization of the ion-polar molecule collision rate constant by trajectory calculations. *J. Chem. Phys.* **1982**, *76*, 5183–5185.

(51) Kosmas, A. M. The average $cos\delta$ approach to the theoretical calculation of thermal energy ion-dipolar molecule reaction rate constant. *J. Physique Lett.* **1984**, *46*, 799–804.

(52) Blanksby, S. J.; Ellison, G. B. Bond Dissociation Energies of Organic Molecules. *Acc. Chem. Res.* **2003**, *36*, 255–263.

(53) Ruscic, B.; Feller, D.; Dixon, D. A.; Peterson, K. A.; Harding, L. B.; Asher, R. L.; Wagner, A. F. Evidence for a Lower Enthalpy of Formation of Hydroxyl Radical and a Lower Gas-Phase Bond Dissociation Energy of Water. *J. Phys. Chem. A* **2001**, *105*, 1–4.

(54) Satta, M.; Gianturco, F.; Carelli, F.; Wester, R. A quantum study of the chemical formation of cyano anions in inner cores and diffuse regions of interstellar molecular clouds. *Astrophys. J.* **2015**, *799*, 228.

(55) Egorov, D.; Schwob, L.; Lalande, M.; Hoekstra, R.; Schlatholter, T. Near edge X-ray absorption mass spectrometry of gas phase proteins: the influence of protein size. *Phys. Chem. Chem. Phys.* **2016**, *18*, 26213–26223.

(56) Solling, T. I.; Kuhlman, T. S.; Stephansen, A. B.; Klein, L. B.; Moller, K. B. The Non-Ergodic Nature of Internal Conversion. *ChemPhysChem* **2014**, *15*, 249–259.

(57) Bernstein, E. R., Ed. *Chemical Reactions in Clusters*; Topics in Physical Chemistry; Oxford University Press: Oxford, New York, 1996; p 158.

(58) Viggiano, A. A.; Morris, R. A.; Paschkewitz, J. S.; Paulson, J. F. Kinetics of the Gas-Phase Reactions of Cl with CH_3Br and CD_3Br: Experimental Evidence for Non-statistical Behavior. *J. Am. Chem. Soc.* **1992**, *114*, 10477–10482.

(59) Liu, J.; Anderson, S. L. Dynamical control of 'statistical' ion-molecule reactions. *Int. J. Mass Spectrom.* **2005**, *241*, 173–184.

(60) Fernandez-Ramos, A.; Miller, J. A.; Klippenstein, S. J.; Truhlar, D. G. Modeling the Kinetics of Bimolecular Reactions. *Chem. Rev.* **2006**, *106*, 4518.

(61) Miller, J. A.; Garrett, B. C. Quantifying the Non-RRKM Effect in the$H+O_2 \rightleftharpoons OH+O$ Reaction. *Int. J. Chem. Kinet.* **1997**, *29*, 275–287.

(62) Miller, J. A.; Klippenstein, S. J. Angular Momentum Conservation in the $O + OH \rightleftharpoons O_2 + H$ Reaction. *Int. J. Chem. Kinet.* **1999**, *31*, 753–756.

(63) Federer, W.; Villingen, H.; Tosi, P.; Bassi, D.; Fergusson, E.; Lindinger, W. In *Astrophysics - State of the Art and Future Directions*; Diercksen, G. H. F., et al.,, Eds.; Eds.; Reidel: Boston, 1985.

(64) Weisentstein, D. K.; Yue, G. K.; Ko, M. K. W.; Sze, N. R. J. M.; Scott, C. J. A two-dimensional model of sulfur species and aerosols. *J. Geophys. Res.* **1997**, *13*, 019–035.

(65) Carlotti, M.; Ade, P. A. R.; Carli, B.; Chipperfield, M.; Hamilton, P. A.; Mencaraglia, F.; Nolt, I.; Ridolfi, M. Diurnal variability and night detection of stratospheric hydroxyl radical from far infrared emission measurements. *Journal of Atmospheric and Solar Terrestrial Physics* **2001**, *63*, 1509–1518.

(66) Green, J. R. et al. Rates of Wintertime Atmospheric SO_2 Oxidation based on Aircraft Observations during Clear Sky Conditions over the Eastern United States. *Journal of Geophysical Research: Atmospheres* **2019**, *124*, 6630–6649.

(67) Smith, J. P.; Dykema, J. A.; Keith, D. W. Production of Sulfates Onboard an Aircraft: Implications for the Cost and Feasibility of Stratospheric Solar Geoengineering. *Earth and Space Science* **2018**, *5*, 150–162.

(68) *Handbook of ATMOSPHERIC ELECTRODYNAMICS Volume I*; Taylor and Francis, 1995; Chapter 1.

(69) Cartoni, A.; Casavola, A. R.; Bolognesi, P.; Borocci, S.; Avaldi, L. VUV Photofragmentation of CH_2I_2: The $[CH_2I - I]^+$ Iso-diiodomethane Intermediate in the I-Loss Channel from $[CH_2I_2]$. *J. Phys. Chem. A* **2015**, *119*, 3704–3709.

(70) Cartoni, A.; Bolognesi, P.; Fainelli, E.; Avaldi, L. Photofragmentation spectra of halogenated methanes in the VUV photon energy range. *J. Chem. Phys* **2014**, *140*, 184307.

(71) Cartoni, A.; Casavola, A. R.; Bolognesi, P.; Castrovilli, M. C.; Catone, D.; Chiarinelli, J.; Richter, R.; Avaldi, L. Insights into 2- and 4(5)-Nitroimidazole Decomposition into Relevant Ions and Molecules Induced by VUV Ionization. *J. Phys. Chem. A* **2018**, *122*, 4031–4041.

(72) Castrovilli, M. C.; Bolognesi, P.; Cartoni, A.; Catone, D.; P., O.; Casavola, A. R.; Turchini, S.; Zema, N.; Avaldi, L. Photofragmentation of halogenated pyrimidine molecules in the VUV range. *J. Am. Soc. Mass Spectrom.* **2014**, *25*, 351–367.

(73) Satta, M.; Bolognesi, P.; Cartoni, A.; Casavola, A. R.; Catone, D.; Markus, P.; Avaldi, L. A joint theoretical and experimental study on diiodomethane: Ions and neutrals in the gas phase. *J. Chem. Phys.* **2015**, *143*, 244312.

(74) Marr, G. V.; West, J. B. Absolute photoionization cross-section tables for helium, neon, argon, and krypton in the VUV spectral regions. *At. Data Nucl. Data Tables* **1976**, *18*, 497–508.

(75) Becke, A. D. Density-functional thermochemistry. III. The role of exact exchange. *J. Chem. Phys.* **1993**, *98*, 5648–5652.

(76) Lee, C.; Yang, W.; Parr, R. G. Development of the Colle-Salvetti correlation-energy formula into a functional of the electron density. *Phys. Rev. B* **1988**, *37*, 785–789.

(77) Vosko, S. H.; Wilk, L.; Nusair, M. Accurate spin-dependent electron liquid correlation energies for local spin density calculations: a critical analysis. *Can. J. Phys.* **1980**, *58*, 1200–1211.

(78) Stephens, P. J.; Devlin, F. J.; Chabalowski, C. F.; Frisch, M. J. Ab Initio Calculation of Vibrational Absorption and Circular Dichroism Spectra Using Density Functional Force Fields. *J. Phys. Chem.* **1994**, *98*, 11623–11627.

(79) Hariharan, P.; Pople, J. A. The influence of polarization functions on molecular orbital hydrogenation energies. *Theor. Chim. Acta* **1973**, *28*, 213.

(80) Francl, M. M.; Pietro, W. J.; Hehre, W. J.; Binkley, J. S.; Gordon, M. S.; DeFrees, D. J.; Pople, J. A. Selfconsistent molecular orbital methods. XXIII. A polarizationtype basis set for second row elements. *J. Chem. Phys.* **1982**, *77*, 3654.

(81) Alecu, M.; Zheng, J.; Zhao, Y.; Truhlar, D. G. Computational Thermochemistry: Scale Factor Databases and Scale Factors for Vibrational Frequencies Obtained from Electronic Model. *J. Chem. Comp. Theory Comput.* **2010**, *6*, 2872.

(82) Mulliken, R. S. Electronic Population Analysis on LCAO-MO Molecular Wave Functions. I. *J. Chem Phys.* **1955**, *23*, 1833–1840.

(83) Frisch, M. J. et al. *Gaussian 09, Revision A.02*; 2016.